ACS Photonics

pubs.acs.org/journal/apchd5

Article

Metasurfaces for Enhancing Light Absorption in Thermoelectric Photodetectors

Nityanand Sharma, Jonathan Bar-David, Noa Mazurski, and Uriel Levy*

Cite This: https://dx.doi.org/10.1021/acsphotonics.0c00691

Read Online

ACCESS | Metrics & More | Article Recommendations | Supporting Information

ABSTRACT: Metasurfaces can be used to enhance the absorption in metallic and dielectric thin films. Taking advantage of this property, we experimentally demonstrate the use of a commercially available thermoelectric device as a thermoelectric photodetector by integrating it with a metallic metasurface array operating as an absorption enhancer for both the visible and the short-wave infrared. Electrical measurement shows that the responsivity of the nanostructured region is an order of magnitude higher than the flat film region. The absorption spectrum and correspondingly the spectral response of the device can be tailored by optimizing the metasurface dimensions. As such, the device can be used as a multiband photodetector for diverse applications.

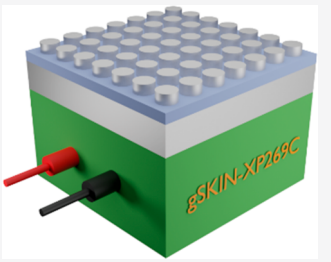

KEYWORDS: *metasurfaces, FIB, thermoelectric, SWIR, enhanced absorption*

The detection of light in the broad spectral regime ranging from the visible to the short-wave infrared has gained renewed attention in the past decade. Among many types of devices, thermoelectric devices[1−4] have been utilized by exploiting their capability to transduce between thermal and electrical signals. Electromagnetic radiation absorbed by these devices is converted to heat, thereby raising the temperature of the device. Subsequently, this rise in temperature creates an electrical current flow, whose scale is dependent on the Seebeck coefficients of the thermoelectric materials used to construct the junction. Incorporating a thin light-absorbing layer, thermoelectric devices can be used as photodetectors. Indeed, such devices have been used for detecting light in the visible region[4,5] and the near-infrared region[6] individually. To enhance the absorption of light within a thermoelectric device, nanostructures can be used.[7−9] By controlling the size and geometrical shapes of the nanostructures, it has been shown to provide efficient light to heat conversion, selection of the desired region for detection of light from narrowband to broadband,[10−16] and counterfeit protection by encoding multiple sets of information[17] as well as generate darkfield colors[18] among others. The typical response time of such a photodetector is in the order of seconds.[19]

In this work, we report on a broadband thermoelectric photodetector operating in the visible and the short-wave infrared based on a commercial thermoelectric device, combined with a nanostructured metasurface array on top of a thin absorber layer. We have used focused ion beam milling to fabricate the nanostructures directly on top of the polished surface of the device. This hybrid device exhibits a linear response and response times in the range of a fraction of seconds, with an order of magnitude enhancement in responsivity as compared with a flat metallic film.

RESULTS AND DISCUSSION

Figure 1 shows the schematic illustration of our fabricated nanostructured broadband light absorber on top of the commercial thermoelectric device. This absorption structure consists of a metal−insulator−metal (MIM) multilayer

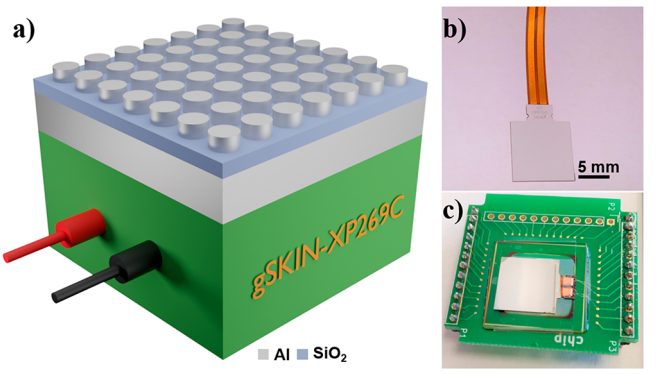

Figure 1. (a) Schematic illustration of the fabricated nanostructured broadband light absorber on top of the commercial thermoelectric device. (b) Image of the commercial device (gSKIN XP 26 9C) before polishing and (c) image of the commercial device after fabrication of the nanostructure on top of the thin absorber layer and wire-bonded for electrical measurements. The dimension of the commercial device is 10 mm × 10 mm × 0.5 mm.

Received: April 27, 2020
Published: July 28, 2020

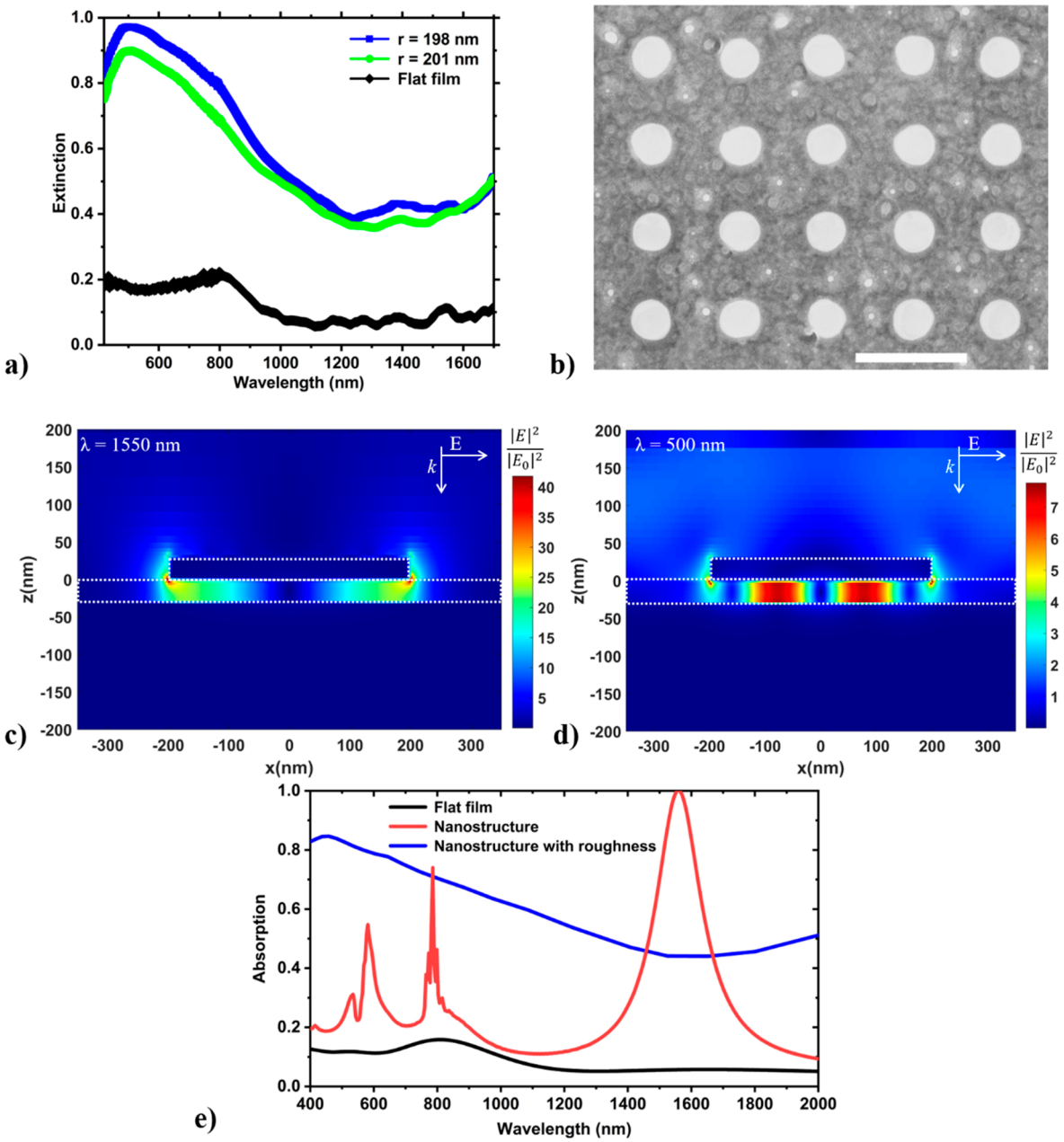

Figure 2. (a) Measured extinction spectra in the visible and short-wave infrared region for a flat film and for two nanostructured areas with disk radii of r = 198 and 201 nm. (b) Scanning electron microscope (SEM) image of a metasurface array with disk radius r = 198 nm and period ∼770 nm. The scale bar is 1 μm. Calculated near field distribution of the electric field intensity $|E/E_0|^2$ being normalized with that of the incident plane wave for a nanostructured disk geometry at a wavelength of (c) λ = 1550 nm and (d) λ = 500 nm. (e) Simulated extinction spectra for a flat film, nanostructure, and nanostructure with surface roughness.

structure.[6] The thickness of the top and the bottom metal layer (aluminum) is 30 and 100 nm, respectively. The insulator layer of SiO_2, with a thickness of 30 nm, separates the two metallic layers (Figure 1a). The multilayer structure is fabricated on top of a polished aluminum surface of the commercial thermoelectric device. Figure 1b shows the thermoelectric device "as is", i.e., before the fabrication of the nanostructures, while Figure 1c shows the device after fabrication and integration with an electrical board.

In the top metallic layer, we have patterned a 70 μm × 70 μm area of nanostructures with varying radii (198 and 201 nm) and a fixed period of ∼770 nm using FIB. Reflection measurements were taken using an inverted microscope equipped with an objective (Nikon, 50×, NA = 0.50) for illuminating the patterned area and collecting the reflected light. Reflected light for the visible and short-wave infrared region was analyzed using Horiba and Ocean optics 4000 spectrometers, respectively. A fiber-coupled tungsten light source (BPS101, B&W Tek) providing light in the spectral range from 350 to 2600 nm, suitable for visible and short-wave infrared region spectroscopic applications, was used as a light source to illuminate the sample.

The measured extinction (calculated by Ext = 1 − R, where R is the normalized reflection spectra) is shown in Figure 2a. As can be seen, an extinction peak of about 95% is obtained around 495 nm (with a minor spectral shift between the

https://dx.doi.org/10.1021/acsphotonics.0c00691
ACS Photonics XXXX, XXX, XXX−XXX

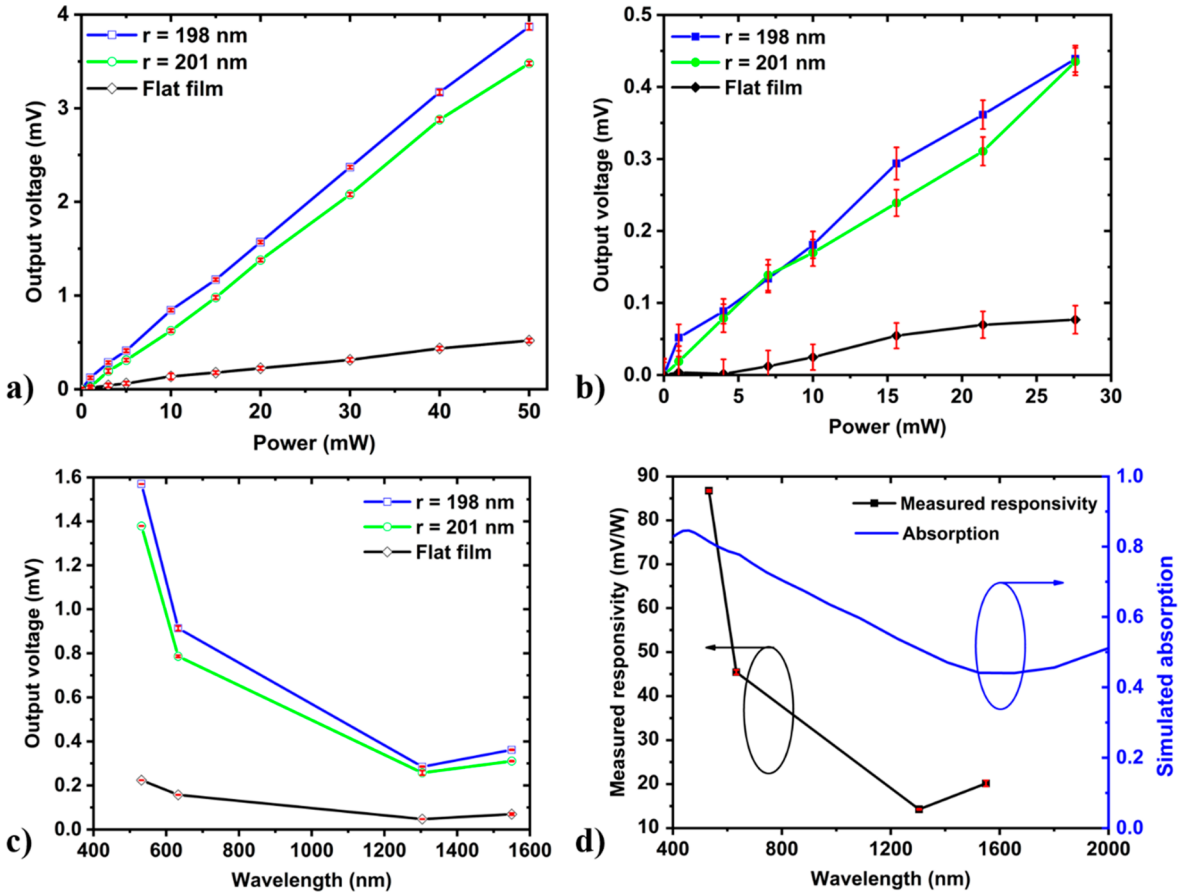

Figure 3. Voltage output of the device as a function of the irradiation power of the laser with a wavelength of (a) 532 nm and (b) 1550 nm. (c) Spectral response of the absorber at different wavelengths (532, 632.8, 1304, and 1550 nm) at a fixed laser output power of 20 mW. (d) The measured spectral responsivity of the absorber with r = 198 nm (black) and the simulated absorption profile for the nanostructures with roughness (blue). Lines are guided for the eye.

different samples of different radii), with decreasing extinction toward longer wavelengths. Figure 2b shows a scanning electron microscope (SEM) image of the nanodisk array fabricated using FIB with a radius of 198 nm and a period of ~770 nm.

A perfect absorber means that transmission and reflection are both close to zero. Zero reflection is achieved when the impedance of the absorbing layer matches that of the free space. The top metallic layer should be sufficiently thin to allow the impinging light to couple into the MIM system. As a result of this coupling, the light gets trapped inside the structure, which leads to maximum absorption. For zero transmission, we chose the bottom layer to be sufficiently thick to completely block the transmission. A detailed discussion on impedance matching and optimization in MIM layers can be seen in the literature.[20,21]

The experimental data were verified by simulating the absorption spectrum using a finite difference time domain (FDTD, Lumerical Inc.) for the investigated nanostructured geometry. Three different sets of simulations were performed to obtain the extinction spectra corresponding to the case of flat films, nanostructures, and nanostructures with surface roughness. The nanostructure cell consists of a metal−insulator−metal (MIM) geometry, where a layer of silicon oxide was sandwiched between the bottom unpatterned aluminum layer and top nanostructured aluminum. A unit cell with a width equal to the period was used, and antisymmetric and symmetric boundary conditions in x- and y-axes were applied. In the z-direction, a perfectly matched layer was placed at a distance of 0.5 μm above and below the MIM layer. A reflection monitor was placed 0.7 μm above the top nanostructured aluminum. Aluminum has been selected as the metal of choice due to its compatibility with the CMOS process. In our simulation, the wavelength-dependent refractive index of Al and SiO_2 was chosen from the FDTD software database. Modeling of nanostructures with surface roughness requires an understanding of surface morphology. To do so, we have extracted the surface morphology from the atomic force microscope (AFM) measurements and imposed it on the surface. The extracted value of the roughness amplitude is ~71 nm with a 2D-correlation length of ~161 nm. The use of Al and SiO_2 allows the excitation of a plasmonic mode at short wavelengths. It is important to note that the wavelength dependent refractive index for the nanostructure with surface roughness may behave differently than the aluminum film.

The simulated extinction spectra presented in Figure 2e for the flat film (black curve) and the nanostructures with surface roughness (blue curve) qualitatively agree with those measured experimentally (Figure 2a). For the nanostructure, the simulation predicts a strong extinction peak in a short-wave infrared region and two relatively weaker peaks in the visible region. The strong electric field confinement occurs at a wavelength of λ = 1550 nm (Figure 2c) and relatively weaker confinement at λ = 500 nm (Figure 2d). For the

https://dx.doi.org/10.1021/acsphotonics.0c00691
ACS Photonics XXXX, XXX, XXX−XXX

nanostructures with surface roughness, the extinction peak occurs around λ = 500 nm and shows a broadband profile extending from the visible to short-wave infrared region. The presence of surface roughness has been reported for enhancing and broadening the extinction profile.[22,23] This broadening can also be attributed to the fact that, during the FIB milling, the ion beam creates perforation onto the sandwiched layers which can further change the optical properties. Fabrication of nanostructures in the top metallic layer of the MIM system using the FIB milling creates a rough surface, as can be seen in the surface morphology image recorded by AFM (Supporting Information Figure S2). In general, fabricated metasurfaces have inaccuracies (leading to inhomogeneity in the structure) and roughness in the scale of nanometers. Since the surface roughness affects the far-field response and the surface features influence the near-field enhancement, it is justifiable to expect that the imperfection intruded in and around nanostructures will modify the extinction spectra.[24] Decreasing extinction spectra toward the longer wavelength can be attributed to the fact that at longer wavelength diffuse reflection dominates.[25] Numerical results for a rise in temperature as a result of being irradiated with the laser beam on metasurfaces and flat film on the top surface of the device are shown in Supporting Information Figure S1.

Following the study of extinction spectra, we have measured the responsivity of the fabricated devices. For these measurements, we have irradiated the fabricated devices at four different wavelengths, two in the visible (λ = 532 nm, red laser λ = 632.8 nm) and the other two in the short-wave infrared (λ = 1304 and 1550 nm), respectively. Irradiation on the absorber area has been performed for 30 s, long enough to ensure that the voltage output reaches its steady-state value. The irradiated area is approximately 30 μm in diameter. We have gradually increased the laser intensity from 0 to 50 mW and measured the voltage extracted by the thermoelectric device. The laser power was adjusted using current. The voltage output from the sensor in response to the laser irradiation was recorded using an oscilloscope (InfiniiVision, Keysight Technologies).

Figure 3a,b shows the measured output voltage (V) of the device as a function of irradiation power (mW) with different radii and for the flat film for wavelengths of 532 and 1550 nm, respectively. The measured output voltage decreases as we shift from the visible to the short-wave infrared region across the different absorber areas for a fixed irradiation power of 20 mW, as shown in Figure 3c. As can be seen, the measured output voltage for the short infrared region is significantly smaller than the visible region. The device shows a linear response as a function of irradiation power for all of the wavelengths. In the absence of the nanostructured absorber area, the responsivity of the flat film is about 8.1 mV/W for a wavelength of 532 nm. In comparison, the absorber area shows a large enhancement in responsivity. The absorber area with r = 198 nm and r = 201 nm shows a responsivity of 86.7 and 80.1 mV/W, respectively, corresponding to a 10.7- and 9.9-fold enhancement. Such responsivity is comparable to the one obtained by making an absorber using a hexagonal array.[26] Measured responsivity on an area with r = 198 nm shows a decreasing trend as we shift from the visible to the short-wave infrared region (Figure 3d). This trend is consistent with the numerically obtained absorption profile of the nanostructures with roughness. As we improve the responsivity in about an order of magnitude, we are expecting to improve the detectivity by an order of magnitude as well. And indeed, we have observed an order of magnitude reduction in the minimal power that can be detected by our device as compared to the unpatterned region.

The response time of the device has been measured by modulating a laser of 56 mW optical power at a wavelength of 532 nm and feeding the generated signal to an oscilloscope (Figure 4). From this measurement, we can obtain the steady-state voltage and the response time, τ, of the device, defined as the time during which the output voltage reaches (1 − 1/e) of its steady-state value, V_{steady}. For each area, we record at least seven cycles of illumination in order to improve the accuracy of the time-constant (response time) measurement. The extracted fall time response from Figure 4 (peak to RMS) is about 200 ms, about 3.4 times faster than the device specifications of 0.7 s. The fabricated device shows about a 25% faster response time in comparison to the unpatterned region. As the response time is dependent on the material and chosen geometry,[27] this faster response can be the result of a small volume of nanostructures.

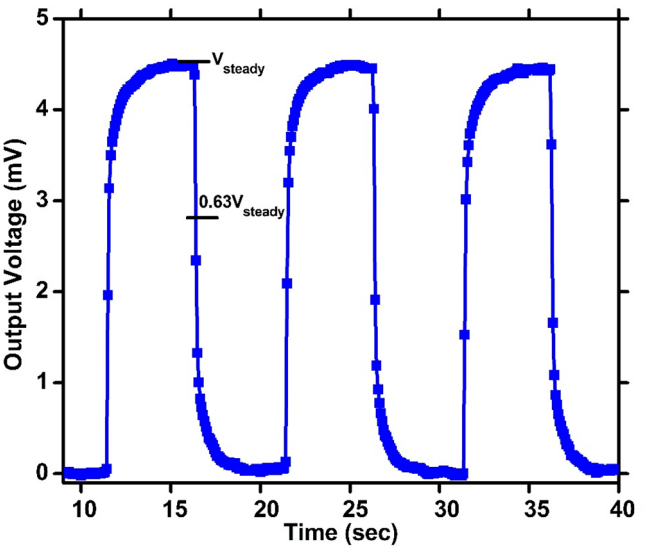

Figure 4. Measured output voltage as a function of time with a constant input optical power of 56 mW at a wavelength of 532 nm.

CONCLUSIONS

We have fabricated a metasurface consisting of a nanostructured metal−insulator−metal broadband super absorber on top of a commercial photoelectric device and have shown that it can be used as a photodetector with an order of magnitude enhancement in the photoresponsivity in the visible and about 7-fold enhancement in the short-wave infrared as compared to a flat film device. The enhancement in photoresponsivity is attributed to the implementation of the nanostructured absorber that allows for enhanced absorption of light over a broadband spectrum in the visible and the short-wave infrared. A response time of about 200 ms was measured. Milling of metasurfaces using FIB allows us to fabricate several areas on a single device by tuning the geometrical parameters. To harness this intriguing enhancement concept, the demonstrated device may be used for cost-effective photosensors over a broad spectral range with diverse applications. As a final point, one may wonder what is the justification of using a lithographically patterned surface instead of applying a simpler approach such as applying a thin layer of matte black

https://dx.doi.org/10.1021/acsphotonics.0c00691
ACS Photonics XXXX, XXX, XXX−XXX

paint or VANTAblack paint for total absorption of light. It is important to note that, while such approaches indeed provide high absorption, the paint is typically much thicker than the thin metasurface absorber, leading to a drastic change in thermal response and time response of the device. Furthermore, most of these paints contain organic compounds, that may cause contamination and damage to the electrical properties of the device. Additionally, paints such as VANTAblack require a high processing temperature, much beyond the allowed temperature range of the device. Costwise, some of these paints are fairly expensive, jeopardizing the concept of achieving a low cost device. Finally, it is rare to find a paint that will be completely black in both the VIS and SWIR regimes. For all of these reasons, our approach offers a significant advantage in realizing the next generation thermoelectric photodetectors.

MATERIALS AND METHODS

Specification of the Device. The thermoelectric device (gSKIN XP 26 9C) was purchased from greenTEG AG. The device has a sensing area dimension of 10 mm × 10 mm × 0.5 mm. The top and bottom sides of the device have 100 μm thick aluminum. The response time of this commercial device is 0.7 s.

Device Polishing. The surface of the commercial thermoelectric device has a roughness in the order of 0.5 μm. Therefore, in order to use it for further fabrication steps, its top surface was lapped and polished to get a flat surface. Approximately 40 μm of bulk aluminum was removed by lapping and polishing.

Lapping. The commercial device was first lapped with diamond pads of size 6 and 1 μm for 30 and 6 min, respectively, with an rpm of 60 and 20. Subsequently, the surface was lapped with a diamond pad of size 0.01 μm for 5 min with an rpm of 10. After the completion of the lapping step, 20 μm thickness was reduced.

Polishing. The lapped surface of the device was then polished with an Al_2O_3 pad of size 0.05 μm for 10 min with an rpm of 10. After that, a colloidal Al_2O_3 slurry of size 0.05 μm was used for delicate polishing for 30 min with an rpm of 10. In the final step of fine polishing, the Al_2O_3 pad of size 0.005 μm was used for 7 min with an rpm of 10. Finally, the device was rinsed with deionized water for 1 min. The polished device has a roughness of 30 ± 3.45 nm.

Fabrication of Metasurfaces. The polished device was coated with metal and dielectric to make it a metal−insulator−metal (MIM) multilayer structure. First, the bottom reflector layer was sputtered with 100 nm thick aluminum (Al) metal, and then, 30 nm of dielectric SiO_2 was deposited using a chemical vapor deposition method. Finally, 30 nm of the top Al layer was sputtered. The nanostructured absorber was fabricated on the top sputtered Al layer using FIB milling. An array of a disk with a pitch of 770 nm and a depth of 30 nm on the sample area of 70 μm × 70 μm was fabricated. The milling current used in fabrication was 430 pA with an accelerating voltage of 30 kV. The depth of milled material was optimized using the number of passes. The optimized number of passes used was 195.

Optical Measurements. Reflection measurement was done using an inverted microscope in air. The microscope was equipped with an objective (50×, Nikon, NA 0.50) for illuminating the sample and collecting the reflected light. Reflected light for the visible and infrared measurement was analyzed using Horiba and Ocean optics 4000 spectrometers, respectively. The light source used to illuminate the sample was a fiber-coupled constant current tungsten light source (BPS101, B&W Tek) having a spectral output from 350 to 2600 nm, suitable for visible and short-wave infrared spectroscopic applications. The extinction was calculated by Ext = 1 − R, where R is the normalized reflection spectra.

Electrical Measurements. Output voltage from the device was measured by excitation using a laser beam. Wavelengths of the laser beam used for measurement were 532, 632, 1304, and 1550 nm. Laser output power was adjusted by adjusting the current through the diode. The output voltage was measured using an oscilloscope (InfiniiVision, Keysight Technologies). For the response time calculation, we measured the voltage as a function of time. From this time-trace plot, we extracted the steady-state voltage (V_{steady}) and the response time, t, of the device, defined as the time during which the output voltage reaches $(1 - 1/e \approx 0.63)$ of its steady-state value, V_{steady}. In order to improve the accuracy of the response time measurements, we measured seven cycles of illumination. All measurements were performed at room temperature under normal ambient conditions.

ASSOCIATED CONTENT

Supporting Information

The Supporting Information is available free of charge at https://pubs.acs.org/doi/10.1021/acsphotonics.0c00691.

Details about the temperature profile of the metasurface and the flat film and surface morphology information (PDF)

AUTHOR INFORMATION

Corresponding Author

Uriel Levy − *Department of Applied Physics, Faculty of Science and The Center for Nanoscience and Nanotechnology, The Hebrew University of Jerusalem, Jerusalem 9190401, Israel;* orcid.org/0000-0002-5918-1876; Email: ulevy@mail.huji.ac.il

Authors

Nityanand Sharma − *Department of Applied Physics, Faculty of Science and The Center for Nanoscience and Nanotechnology, The Hebrew University of Jerusalem, Jerusalem 9190401, Israel;* orcid.org/0000-0001-7397-0508

Jonathan Bar-David − *Department of Applied Physics, Faculty of Science and The Center for Nanoscience and Nanotechnology, The Hebrew University of Jerusalem, Jerusalem 9190401, Israel;* orcid.org/0000-0002-4464-636X

Noa Mazurski − *Department of Applied Physics, Faculty of Science and The Center for Nanoscience and Nanotechnology, The Hebrew University of Jerusalem, Jerusalem 9190401, Israel*

Complete contact information is available at: https://pubs.acs.org/10.1021/acsphotonics.0c00691

Notes

The authors declare no competing financial interest.

ACKNOWLEDGMENTS

The research was supported by the Israeli Ministry of Science and Technology.

REFERENCES

(1) Venkatasubramanian, R.; Siivola, E.; Colpitts, T.; O'Quinn, B. Thin-Film Thermoelectric Devices with High Room-Temperature Figures of Merit. *Nature* **2001**, *413* (6856), 597−602.

(2) Birkholz, U.; Fettig, R.; Rosenzweig, J. Fast Semiconductor Thermoelectric Devices. *Sens. Actuators* **1987**, *12* (2), 179−184.

(3) Modarres-Zadeh, M. J.; Abdolvand, R. High-Responsivity Thermoelectric Infrared Detectors with Stand-Alone Sub-Micrometer Polysilicon Wires. *J. Micromech. Microeng.* **2014**, *24* (12), 125013.

(4) Monshat, H.; Liu, L.; Lu, M. A Narrowband Photo-Thermoelectric Detector Using Photonic Crystal. *Adv. Opt. Mater.* **2019**, *7* (3), 1801248.

(5) Mudachathi, R.; Tanaka, T. Broadband Plasmonic Perfect Light Absorber in the Visible Spectrum for Solar Cell Applications. *Adv. Nat. Sci.: Nanosci. Nanotechnol.* **2018**, *9*, 015010.

(6) Liu, N.; Mesch, M.; Weiss, T.; Hentschel, M.; Giessen, H. Infrared Perfect Absorber and Its Application As Plasmonic Sensor. *Nano Lett.* **2010**, *10* (7), 2342−2348.

(7) Coppens, Z. J.; Li, W.; Walker, D. G.; Valentine, J. G. Probing and Controlling Photothermal Heat Generation in Plasmonic Nanostructures. *Nano Lett.* **2013**, *13* (3), 1023−1028.

(8) Kubo, W.; Kondo, M.; Miwa, K. Quantitative Analysis of the Plasmonic Photo-Thermoelectric Phenomenon. *J. Phys. Chem. C* **2019**, *123* (35), 21670−21675.

(9) Miwa, K.; Ebihara, H.; Fang, X.; Kubo, W. Photo-Thermoelectric Conversion of Plasmonic Nanohole Array. *Appl. Sci.* **2020**, *10* (8), 2681.

(10) Aydin, K.; Ferry, V. E.; Briggs, R. M.; Atwater, H. A. Broadband Polarization-Independent Resonant Light Absorption Using Ultrathin Plasmonic Super Absorbers. *Nat. Commun.* **2011**, *2* (1), 517.

(11) Hao, J.; Wang, J.; Liu, X.; Padilla, W. J.; Zhou, L.; Qiu, M. High Performance Optical Absorber Based on a Plasmonic Metamaterial. *Appl. Phys. Lett.* **2010**, *96* (25), 251104.

(12) Hao, J.; Zhou, L.; Qiu, M. Nearly Total Absorption of Light and Heat Generation by Plasmonic Metamaterials. *Phys. Rev. B: Condens. Matter Mater. Phys.* **2011**, *83* (16), 165107.

(13) Butun, S.; Aydin, K. Structurally Tunable Resonant Absorption Bands in Ultrathin Broadband Plasmonic Absorbers. *Opt. Express* **2014**, *22* (16), 19457.

(14) Cui, Y.; Fung, K. H.; Xu, J.; Ma, H.; Jin, Y.; He, S.; Fang, N. X. Ultrabroadband Light Absorption by a Sawtooth Anisotropic Metamaterial Slab. *Nano Lett.* **2012**, *12* (3), 1443−1447.

(15) Zhang, B.; Zhao, Y.; Hao, Q.; Kiraly, B.; Khoo, I.-C.; Chen, S.; Huang, T. J. Polarization-Independent Dual-Band Infrared Perfect Absorber Based on a Metal-Dielectric-Metal Elliptical Nanodisk Array. *Opt. Express* **2011**, *19* (16), 15221.

(16) Lei, L.; Li, S.; Huang, H.; Tao, K.; Xu, P. Ultra-Broadband Absorber from Visible to near-Infrared Using Plasmonic Metamaterial. *Opt. Express* **2018**, *26* (5), 5686.

(17) Ng, R. J. H.; Krishnan, R. V.; Dong, Z.; Ho, J.; Liu, H.; Ruan, Q.; Pey, K. L.; Yang, J. K. W. Micro-Tags for Art: Covert Visible and Infrared Images Using Gap Plasmons in Native Aluminum Oxide. *Opt. Mater. Express* **2019**, *9* (2), 788.

(18) Ng, R. J. H.; Krishnan, R. V.; Wang, H.; Yang, J. K. W. Darkfield Colors from Multi-Periodic Arrays of Gap Plasmon Resonators. *Nanophotonics* **2020**, *9* (2), 533−545.

(19) Thermal Power Sensors-Thorlabs Product. https://www.thorlabs.com/newgrouppage9.cfm?objectgroup_id=3333.

(20) Aalizadeh, M.; Khavasi, A.; Butun, B.; Ozbay, E. Large-Area, Cost-Effective, Ultra-Broadband Perfect Absorber Utilizing Manganese in Metal-Insulator-Metal Structure. *Sci. Rep.* **2018**, *8* (1), 9162.

(21) Mattiucci, N.; Bloemer, M. J.; Aközbek, N.; D'Aguanno, G. Impedance Matched Thin Metamaterials Make Metals Absorbing. *Sci. Rep.* **2013**, *3* (1), 3203.

(22) Mills, D. L.; Maradudin, A. A. Surface Roughness and the Optical Properties of a Semi-Infinite Material; the Effect of a Dielectric Overlayer. *Phys. Rev. B* **1975**, *12* (8), 2943−2958.

(23) Peiponen, K.-E.; Tsuboi, T. Metal Surface Roughness and Optical Reflectance. *Opt. Laser Technol.* **1990**, *22* (2), 127−130.

(24) Lu, Y.-W.; Li, L.-Y.; Liu, J.-F. Influence of Surface Roughness on Strong Light-Matter Interaction of a Quantum Emitter-Metallic Nanoparticle System. *Sci. Rep.* **2018**, *8* (1), 7115.

(25) Larena, A.; Millán, F.; Verdú, M.; Pinto, G. Surface Roughness Characterisation of Multilayer Polymer Films for Graphic Arts Applications. *Appl. Surf. Sci.* **2001**, *174* (3−4), 217−224.

(26) Pan, Y.; Tagliabue, G.; Eghlidi, H.; Höller, C.; Dröscher, S.; Hong, G.; Poulikakos, D. A Rapid Response Thin-Film Plasmonic-Thermoelectric Light Detector. *Sci. Rep.* **2016**, *6* (1), 37564.

(27) Goupil, C. *Continuum Theory And Modeling of Thermoelectric Elements*; Goupil, C., Ed.; Wiley: 2016.

https://dx.doi.org/10.1021/acsphotonics.0c00691
ACS Photonics XXXX, XXX, XXX−XXX